energies

MDPI

Article

Energy Conversion System and Control of Fuel-Cell and Battery-Based Hybrid Drive for Light Aircraft

Tomasz Miazga [1,*], Grzegorz Iwański [1,*] and Marcin Nikoniuk [2]

[1] Faculty of Electrical Engineering, Warsaw University of Technology, 75, Koszykowa St., 00-662 Warszawa, Poland
[2] Faculty of Transport, Warsaw University of Technology, 75, Koszykowa St., 00-662 Warszawa, Poland; marcin.nikoniuk@pw.edu.pl
* Correspondence: tomasz.miazga@ee.pw.edu.pl (T.M.); iwanskig@isep.pw.edu.pl (G.I.)

Abstract: The paper presents a power electronic conversion system and its control for a fuel cell and a battery-based hybrid drive system for a motor glider. The energy conversion system is designed in such a way that the fuel cell gives power equal to the electric drive power demand for horizontal flight, whereas during motor glider take-off and climbing, the fuel cell is supported by the battery. The paper presents the power demand related to the assumed mission profile, the main components of the hybrid drive system and its holistic structure, and details of power electronics control. Selected stationary experimental test results related to the energy conversion and drive system are shown. Some results related to the aircraft tests on a runway are presented.

Keywords: fuel cell; energy conversion; energy management; power converter; aircraft propulsion

Citation: Miazga, T.; Iwański, G.; Nikoniuk, M. Energy Conversion System and Control of Fuel-Cell and Battery-Based Hybrid Drive for Light Aircraft. *Energies* **2021**, *14*, 1073. https://doi.org/10.3390/en14041073

Academic Editor: Kaushik Rajashekara

Received: 9 December 2020
Accepted: 15 February 2021
Published: 18 February 2021

1. Introduction

Battery electric drives are nowadays intensively developed for road vehicles. In aerospace, they are commonly used in unmanned aerial vehicles. Similar technologies in some range can be taken into consideration for light manned aircrafts such as motor gliders, training aircrafts, or others in which the mission is short. Due to the limited energy density of presently available electrochemical cells, the range of flight can be increased by hydrogen fuel cell systems [1–3] for which energy density, including the weight and volume of fuel cell, hydrogen storage, and supplementary equipment, is higher. However, to avoid the fuel cell system sizing for peak power needed during take-off and climbing, and to design it only for the low power during horizontal flight, it is highly recommended to use a fuel cell as part of a hybrid energy source supported by additional energy storage. The energy storage provides boost power during take-off and climbing and should be sized considering both energy and power demand. In academic research the specific energy of lithium-ion cells reaches 300 Wh/kg [4]. From among commercially available Li-Ion cells specific energy of 100–220 Wh/kg is available, but those of higher specific energy have lower power density. Due to relatively short time of energy storage usage during mission profile, high energy density but low power density cells may not meet the requirements. Even taking into account Li-Ion cells with specific energy value in the mid-range, it is still one order higher than commercially available supercapacitor cells (4–6 Wh/kg).

The hybrid-electric drive system with a fuel cell has been described in a few papers, mainly in terms of fuel cell behavior. As the fuel cell system is the most expensive component in the entire hybrid drive system, its design and optimization is the most challenging [5] issue. Possible direct hybridization without a fully controlled power electronic converter [6] may be considered for small unmanned aerial vehicles. Direct connection of fuel cell and battery terminals does not allow fully controlled energy management, which may cause problems in higher power ranges. In a directly connected fuel cell and battery in a converter-less drive system, load sharing between the fuel cell and battery

depends on the battery discharge level, and depending on the battery voltage level, the fuel cell operates at a different point, one not necessarily optimal in a specific stage of the aircraft mission.

Some of the developed hybrid drive systems with fuel cells for light aircrafts contain DC/DC power electronic converters for both fuel cell and battery [7]. Depending on the power of both devices, such a solution provides voltage matching of the supply devices to the DC bus voltage required by the motor inverter. However, in the case of motor glider, the fuel cell power demanded only for horizontal flight is much smaller than the demanded power of the battery serving as a boosting energy source. At the same time, the battery energy demand makes it possible to design the battery so that the voltage is high enough to connect directly to the DC bus. This way, a relatively large bidirectional DC/DC converter between the battery and the DC bus is avoided. However, if done this way, there is no direct regulation of the battery current and its control is indirect through the use of battery current signal in the fuel cell converter control structure.

The superior control structure (energy management) can be made outside the power converters controllers in the on-board computer, or another external controller which collects the necessary data from the fuel cell, fuel cell DC/DC converter, battery, and load [8]. However, the signal transmission delays and possible faults of the communication network prompted us to find solutions that allow energy management without communication system engagement. This is one of the ways hybrid system reliability increases (elimination of communication system problems as a reason for hybrid drive faults generation). This way, the on-board computer applied in the designed system is responsible for sending starting commands only and is not involved in further control of power converters. It is also used to visualize hybrid drive operation to give some necessary information to the pilot, and for data collection from the experiments, but this does not influence the hybrid drive system operation.

Fault prevention can be achieved in a different way, such as through over-sizing of components, additional protections, redundancy, etc. [9,10]. The proposed solution of communication-less energy management can be treated as a redundant solution to the communication-based system. It must be noted that a communication-based system can have wider functionalities due to the fact that it collects data from all devices simultaneously, but in the case of the communication system fault, an additional energy management method which provides safe control of power converters and assures the demanded power may be of interest during the design of hybrid-electric propulsion not only with a fuel cell system, but also with other types of energy sources.

The paper presents the structure of a power electronics-based energy conversion system and its control for a hybrid drive composed of a 10 kW fuel cell and 30 kW of battery power for a motor glider. Section 2 presents the assumed profile of propeller torque and speed related to the stationary conditions and braking power assumed for different stages of flight. This is followed by the selection of the fuel cell, battery, and motor parameters, meeting the requirements in terms of energy and power demands. Propeller characteristics are also provided. Section 3 presents the selected topologies of DC/DC and DC/AC power converters and their parameters, as well as some discussion about the efficiency of electrical energy conversion depending on the braking power demand. Section 4 presents the communication structure and control method, allowing safe operation in case of communication system fault, followed by some results related to the fuel cell system protection against overload and its intentional short circuiting. Some discussion related to other types of possible faults and concepts of how the conversion system should assist in these states is given. Section 5 presents the experimental tests results for a full profile in stationary conditions using a fuel cell simulator instead of the real unit. Section 6 presents the selected results of experimental tests of the fuel cell and battery-based hybrid drive system in a real motor-glider on a runway.

The main scope of the paper is an alternative control method not involving a communication system in the entire process of the energy conversion unit, which can be used

after any used CAN bus communication faults between the fuel cell controller or between power conversion units.

2. Power System Demands and Components Selection

2.1. Loading Profile

The power electronics converter and its control for a hybrid-electric drive system described in this paper are developed for a motor glider of assumed max. take-off weight 660 kg. Mission profile is divided into the following stages:

- Start-up of the power system (0–30 s)–30 s ramp used
- Taking-off of the motor glider (30–60 s)–maximum mechanical power 37 kW
- Climbing (60–330 s)–mechanical power equal to 33 kW
- Horizontal flight (15 min)–mechanical power equal to 9 kW
- Maneuvering before landing (1 min)–optional
- Landing

Due to the fact that the considered AOS-H2 light aircraft is a glider with relatively high aerodynamic performance, the horizontal flight power demand is significantly smaller than the power demand during take-off and climbing. Figure 1 presents the profile of the demanded torque and rotational speed related to the stationary conditions to obtain the profile of demanded power. It must be noted that the referenced rotational speed for a given propeller characteristic does not take into consideration the characteristic change for different velocities of the aircraft, because most tests have been made in stationary conditions.

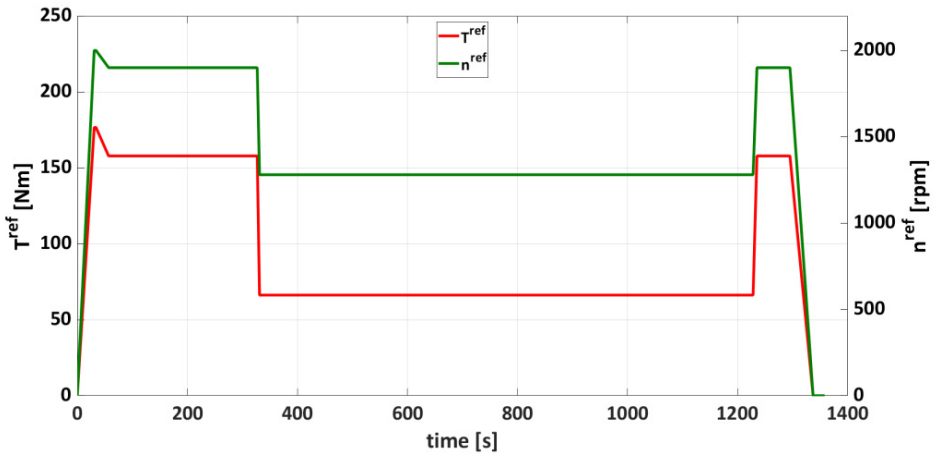

Figure 1. Propeller torque T^{ref} and rotational speed n^{ref} profile for stationary tests of electric drive.

2.2. Fuel Cell Parameters

A 10 kW fuel cell system used in the designed platform suffices to keep the horizontal flight without the use of a battery. The fuel cell unit comprises two H-5000 Horizon's stacks whose construction has been adapted to the airframe. The main parameters of the selected single stack are provided in Table 1. Details of the single original stack are available in the datasheet [11]. Figure 2 presents voltage-current and power-current output characteristics of the single stack.

Table 1. Parameters of the single fuel cell stack.

Symbol	Parameter	Value
P_{FCn}	Rated single stack power	5 kW
U_{FCn}	Rated single stack voltage	72 V
I_{FCn}	Rated stack current	70 A
T_{FC_max}	Max. stack temperature	65 °C
P_{H2}	Hydrogen pressure	0.45–0.55 bar
ε_{FC}	Efficiency at 72 V	40%

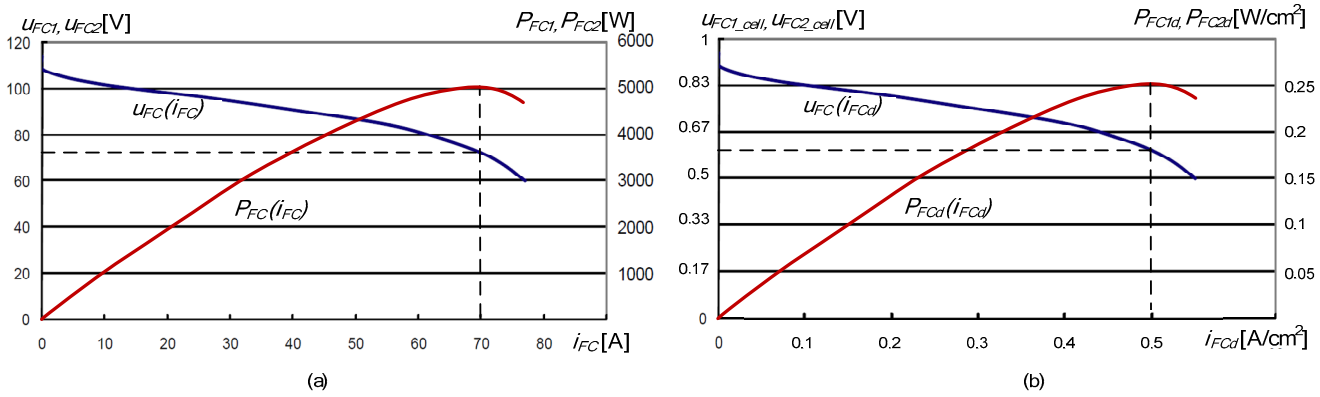

Figure 2. Output characteristics of a single 5kW stack of the fuel cell according to the fuel cell user manual [11]. (**a**) voltage U_{FC} and power P_{FC} for single stack as a functions of fuel cell current I_{FC}, (**b**) voltage of single cell U_{FC_cell} and power density P_{FCd} as a functions of fuel cell current density I_{FCd}.

Detailed properties of the fuel cell system, composed of two series connected stacks designed for this aircraft, can be found in [12]. Total weight of the fuel cell system equals ~65 kg. Fuel cell stacks are periodically short-circuited for tens of milliseconds to improve humidification of membranes [13]. In these conditions, the stack does not provide energy to the load due to the zeroed voltage on the stack terminals, so the energy at this state is consumed from a battery used in a hybrid system.

2.3. Battery Parameters

Taking into account that the fuel cell system is designed for the power range needed to obtain safe horizontal flight, during any other state requiring higher power (e.g., during climbing or maneuvering), the battery set providing boosting energy has to be used. The selected battery pack comprises 96 Lithium-Polymer cells, model SLPB78205130H from Kokam, which is dedicated for automotive, military, and aviation applications. According to [14], the estimated resistance of a single cell equals 4 mΩ. The energy required for five minutes of take-off and climbing and for one minute of maneuvering equals 3 kWh. Additional 2.5 kWh is stored in case of energy deficit from the fuel cell during horizontal flight if the demanded power is higher than the assumed 10 kW and in case of fuel cell system emergency stop, to provide the energy necessary to assure time to find a safe place for landing. The battery system is equipped with its own battery management system BMS (responsible for monitoring each battery cell voltage and temperature, battery voltage, and battery current) and common DC-bus precharging. Parameters of the battery pack are provided in Table 2.

Table 2. Parameters of the battery pack for the AOS-H2 motor glider.

Symbol	Parameter	Value
C_{BAT}	Capacity	16 Ah
	Number of cells	96
E_{BAT}	Nominal energy	5.5 kWh
U_{BAT_max}	Maximum voltage (4.2 V/cell)	403 V
U_{BAT_nom}	Nominal voltage (3.7 V/cell)	355 V
U_{BAT_min}	Minimum voltage (3 V/cell)	288 V
I_{BAT_max}	Maximum discharge current	100 A
R_{BAT}	Battery resistance	384 mΩ [14]
m_{BAT}	Battery weight	65 kg

The minimum voltage for selected cells declared by the manufacturer equals 2.7 V, but to increase the battery lifetime, such deep discharge is avoided by setting the minimum voltage for a single cell at 3 V in a BMS system. Depending on the demanded power, a few

percent of energy stored in the battery will not be used (e.g., 7% at 5 C of discharging current and 10% at 8 C of discharging current). According to short-circuiting of fuel cell stacks, the battery must be resistant to temporarily increased current. This is solved by average current calculation per each 100 ms period, and the battery is disconnected if the current five consecutive samples calculated this way exceed the limit.

2.4. Selection of Electric Motor for Propeller

From the point of view of aircraft design, propeller characteristics of thrust vs. rotational speed and vs. aircraft velocity are the most important issues. However, from the point of view of electric drive system design and control, the power/torque vs. rotational speed characteristics are crucial because they determine energy consumption from both the battery and the fuel cell. The motor-propeller set characteristics obtained in the stationary tests are shown in Figure 3. Maximum mechanical power 38 kW in stationary conditions is available at 1950 rpm of rotational speed. The propeller of 1.85 m diameter is designed in such a way to provide higher thrust for climbing velocity 80–100 km/h (1.7 kN) than in stationary conditions (1kN) at full rotational speed 1950 rpm. Real thrust has not been measured because the aircraft was not equipped with a thrust sensor.

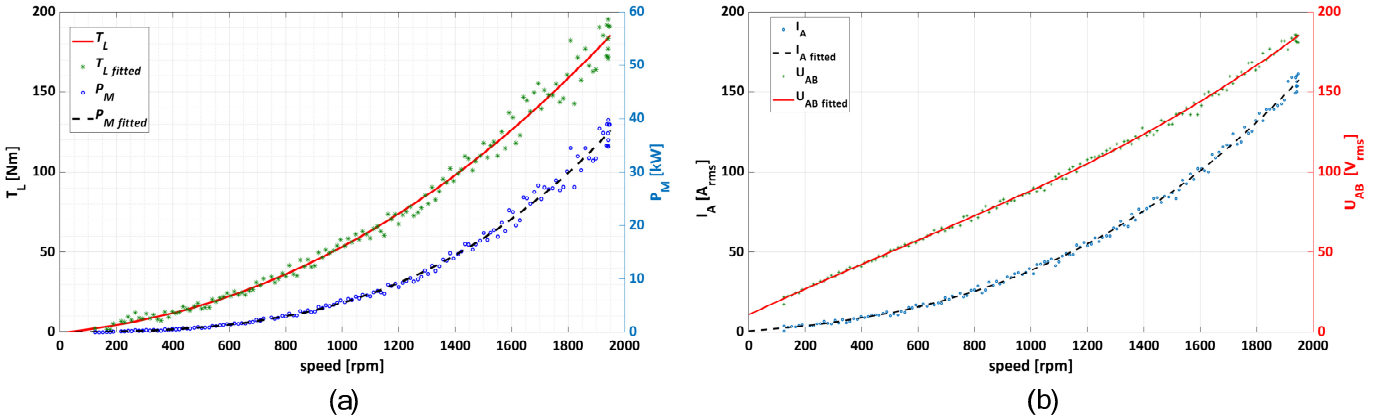

Figure 3. Torque-speed and power speed characteristics of the propeller in stationary conditions (**a**), and motor voltage and current characteristics vs. speed (**b**).

In horizontal flight, the propeller speed is considerably lower than the maximum speed (1300 rpm vs. 1950 rpm respectively), so even a slight change to 1400 rpm or even 1500 rpm is possible. Thus, the voltage required in the DC bus by a DC/AC converter is much lower than battery voltage connected directly to the DC bus. Please note that at the end of the profile, we assumed the optional maneuvering stage before landing, and at this stage, the speed is maximal. Of course, the possibility depends not only on the battery terminal voltage but on the energy available in the battery as well.

The selected motor was EMRAX 268 VHML MVAC, which according to the motor datasheet [15], can provide 40 kW at 2000 rpm. Maximum motor rms line to line voltage for maximum speed equals 180 V and the rms current equals 160 A. It is visible that at low speed (so low mechanical torque), the voltage linearly depends on the speed, while at higher speed, the torque increases according to the speed square function and the stator resistance voltage drop increases; thus, the stator terminal voltage is slightly higher than the one resulting from the linear speed function.

The electric motor has to provide the required torque at a given speed without exceeding the maximum temperature in different ambient conditions. Figure 4 presents the motor temperature measured using a KTY 81/210 embedded winding temperature sensor during the testing profile.

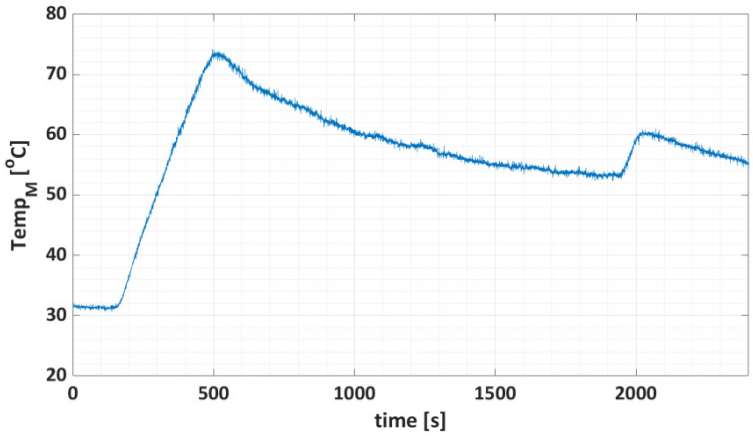

Figure 4. Motor temperature waveform during the testing profile.

It can be seen that the temperature margin allows take-off of the aircraft even after a longer stay on the runway in case of high solar radiation, which may increase significantly the initial temperature of the uncovered motor.

The main parameters of the selected electric motor are provided in Table 3. According to k_ω [rpm/1Vudc) the minimum dc voltage required to obtain 2000 rpm of rotational speed equals 285 V, so it is close to the minimum battery voltage and it makes it possible to almost fully use the energy stored in the battery up to the minimum level of dc (battery) voltage (3 V/cell).

Table 3. Parameters of the air-cooled EMRAX 268 VHML MVAC motor.

Symbol	Parameter	Value
P_M	Maximum continuous mechanical power at 2000 rpm	40 kW
I_M	Maximum continuous stator rms current	190 A
L_d/L_q	Motor inductances	126/118 µH
R_s	Phase resistance at 25 °C	12 mΩ
ε_M	Motor efficiency	0.92–0.98
$Temp_{M\_max}$	Maximum temperature	120 °C
k_ω	Specific load speed	7(rpm/1Vudc)
m_M	Motor weight	20 kg

3. Power Conversion System Structure

3.1. Scheme of the Applied Power Conversion System

The structure of the power conversion system for a hybrid fuel cell and battery-based drive system is presented in Figure 5. During starting-up and climbing, the battery provides higher power than a fuel cell; therefore, the battery is connected directly to the common DC bus. This is to avoid a heavy and bulky 30 kW DC/DC bidirectional converter between the battery and the DC bus.

The typical two-level structure of the DC/AC motor converter was applied due to the relatively small power of the electric drive built with IGBT technology. The DC/DC converter has been designed in silicon carbide technology to increase the operational frequency (switching frequency) to 100 kHz. This provides a significant reduction of size, weight, and volume of passive filter components with a reasonable level of losses. The used transformer-less structure of the power converter has higher efficiency. To make the implementation of this topology possible, the fuel cell voltage has been increased by a series connection of two stacks. It provides 150 V at the maximum power point (nominal power), and higher when the fuel cell is not fully loaded.

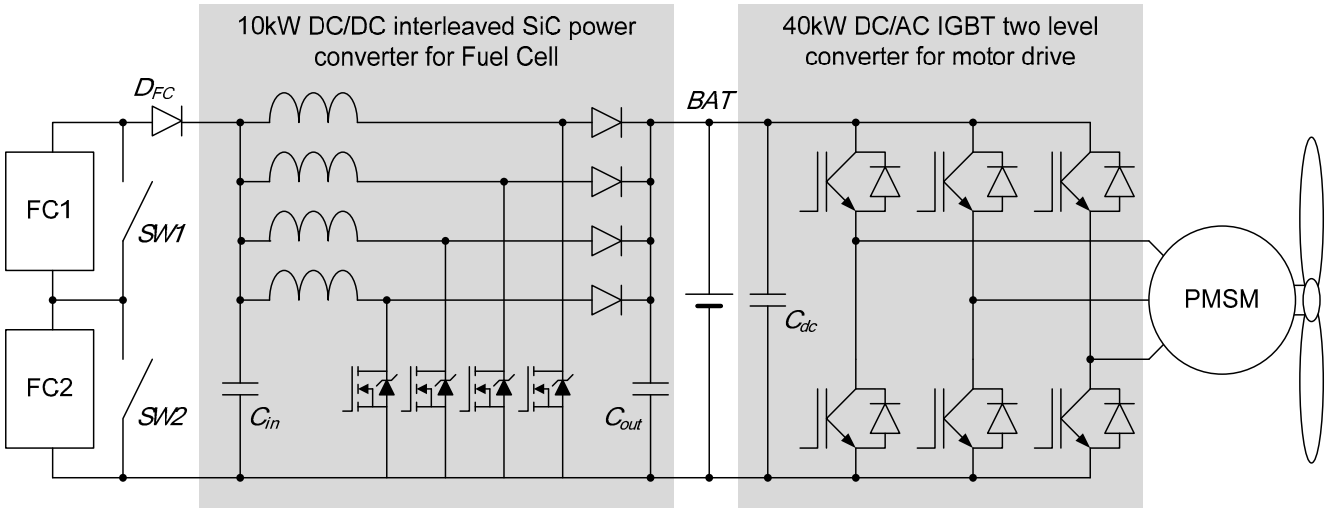

Figure 5. Scheme of the power conversion system with a DC/DC silicon carbide (SiC) power converter responsible for fuel cell loading and DC/AC insulated gate bipolar transistor IGBT converter responsible for feeding the propeller driving a permanent magnet synchronous motor.

3.2. DC/AC IGBT Motor Converter and DC/DC Silicon-Carbide Power Fuel Cell Converter

Insulated gate bipolar transistors (IGBT) are a mature technology [16] mostly used in tens-kW motor drive inverters. The DC/AC power electronic converter for a motor drive is built with SEMiX603GB066HDs modules. The module maximum current is around 2.5 times higher than required by the motor, but the module thermal losses for the desired rms motor phase current are the lowest among modules from the same family (modules with 300 A, 400 A, 600 A of rated current are compared). Therefore, the weight and volume of the heat sink are smaller. This is especially important in the case of the air-cooled converter (this was one of the project requirements). Power modules are switched with 10 kHz frequency, which is enough to obtain high quality, sinusoidal motor current with a low amount of switching frequency harmonics, even if the electric motor frequency at 2000 rpm is relatively high (333 Hz). At the selected switching frequency, the converter efficiency equals 97.6% for full electric power (40 kW) and 96.6% for 10 kW of electric power required during horizontal flight. The main parameters of the motor converter are shown in Table 4. The DC/AC converter is controlled from the control board built with a TMS320F28335 microcontroller with external analog/digital converters. Figure 6a presents a view of the designed and built 40 kW DC/AC power converter.

The DC/DC converter is designed and constructed with DF11MR12W1M1_B11 silicon carbide (SiC) modules. Switching frequency for this converter equals 100 kHz to reduce the weight and volume of passive filters [17,18]. Interleaved topology has been chosen due to possible postfault operation [19] when one of the converter legs fails, but this issue is beyond the scope of this paper. Figure 6b presents the designed and constructed DC/DC converter. Its efficiency equals 99.2% at full power (10 kW). The main parameters of the fuel cell converter are shown in Table 5. To make control of the power converter with this frequency possible, the control board is built with FPGA XILINX XC7A50T-2CSG325I, and with the same DSP microcontroller as in the DC/AC converter, which here is responsible mainly for CAN communication with other devices. The DC/DC converter is equipped with battery current measurement to make it possible to control the battery current during system operation and to make energy management possible without engagement of the communication system.

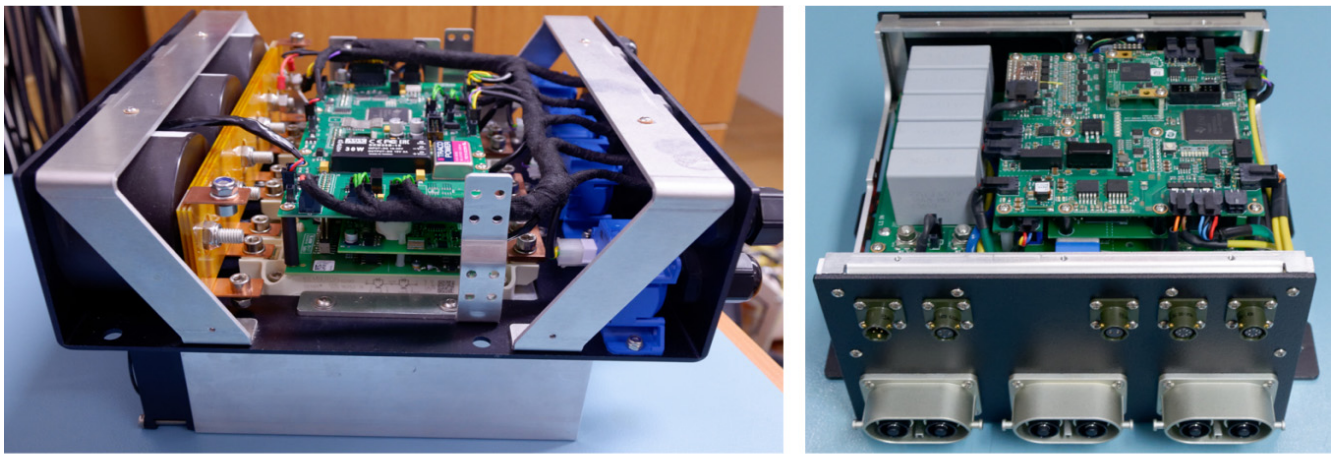

Figure 6. View of (**a**) a DC/AC IGBT air-cooled motor converter and (**b**) a DC/DC silicon carbide air-cooled fuel cell converter.

Table 4. Parameters of the DC/AC motor converter.

Symbol	Parameter	Value
U_{DC_max}	Maximum DC bus voltage	450 V
I_{INV_cont}	Continuous current (rms)	160 A
I_{INV_peak}	Peak current (rms)	320 A
m_{INV}	Weight	13 kg

Table 5. Parameters of the DC/DC fuel cell converter.

Symbol	Parameter	Value
U_{DCDC_max}	Maximum DC bus voltage	450 V
I_{DCDC_max}	Maximum continuous current	67 A
U_{DCDC_in}	Input voltage range	0-U_{DCDC_out}
m_{DCDC}	Weight	4 kg

3.3. Discussion on the Power Conversion System Efficiency

The total efficiency ε_t of electrical energy conversion can be determined as follows. The DC bus electric power P_{eDC} fed to the DC/AC converter is higher than mechanical braking power P_m due to the efficiency of the motor $\varepsilon_{DC/AC}$ and DC/AC converter.

$$P_{eDC} = \frac{P_m}{\varepsilon_{DC/AC}\varepsilon_{PMSM}} \tag{1}$$

Battery power $P_{bat,}$ meant as the sum of power delivered to the DC bus and internal resistance power losses, equals the difference between total DC power P_{eDC} and fuel cell P_{FC} power reduced by DC/DC converter losses divided by battery efficiency.

$$P_{BAT\_total} = \frac{P_{eDC} - P_{FC}\varepsilon_{DC/DC}}{\varepsilon_{BAT}} = \frac{\frac{P_m}{\varepsilon_{DC/AC}\varepsilon_{PMSM}} - P_{FC}\varepsilon_{DC/DC}}{\varepsilon_{BAT}} = \frac{P_m - P_{FC}\varepsilon_{DC/DC}\varepsilon_{DC/AC}\varepsilon_{PMSM}}{\varepsilon_{BAT}\varepsilon_{DC/AC}\varepsilon_{PMSM}} \tag{2}$$

Total efficiency ε_t, meant as the ratio between mechanical power and total electric power delivered by fuel call and battery (including energy losses on the battery internal resistance), can be calculated as follows. Equation (3) considers only electrical energy conversion efficiency without propeller efficiency and without fuel cell efficiency.

$$\varepsilon_t = \frac{P_m}{P_{FC} + P_{BAT}} = \frac{P_m}{P_{FC} + \frac{P_m - P_{FC}\varepsilon_{DC/DC}\varepsilon_{DC/AC}\varepsilon_{PMSM}}{\varepsilon_{BAT}\varepsilon_{DC/AC}\varepsilon_{PMSM}}} = \frac{P_m\varepsilon_{BAT}\varepsilon_{DC/AC}\varepsilon_{PMSM}}{P_m + P_{FC}\varepsilon_{DC/AC}\varepsilon_{PMSM}(\varepsilon_{BAT} - \varepsilon_{DC/DC})} \tag{3}$$

where

$$\varepsilon_{BAT} = \frac{P_{BAT}}{P_{BAT}+I_{BAT}^2 R_{BAT}} = \frac{P_{BAT}}{P_{BAT}+\left(\frac{P_{BAT}}{U_{BAT}}\right)^2 R_{BAT}} = \frac{U_{BAT}^2}{P_{BAT}R_{BAT}+U_{BAT}^2} = \frac{U_{BAT}^2}{\left(\frac{P_m}{\varepsilon_{DC/AC}\varepsilon_{PMSM}}-P_{FC}\varepsilon_{DC/DC}\right)R_{BAT}+U_{BAT}^2} = \frac{U_{BAT}^2}{\left(\frac{P_m-P_{FC}\varepsilon_{DC/DC}\varepsilon_{DC/AC}\varepsilon_{PMSM}}{\varepsilon_{DC/AC}\varepsilon_{PMSM}}\right)R_{BAT}+U_{BAT}^2} \quad (4)$$

and P_{bat} is battery power delivered to the DC bus.

The efficiency map of the electric motor is provided by the manufacturer in the motor datasheet. A separate efficiency test of the electric motor has not been done within the project. It has to be noted that the motor's precise efficiency map must be obtained not with a propeller but with a more stable controlled mechanical load, and this is done by the motor manufacturer. From the efficiency map provided by the manufacturer [15], it can be seen that for speed and torque operating point during take-off and climbing (1900 rpm, 165 Nm (33 kW)), motor efficiency equals 94%, and for horizontal flight (1300 rpm, 65 Nm (9 kW)) it equals 87%. Considering that the motor efficiency for the horizontal flight is about 87%, 10kW of fuel cell power is marginally enough, but considering that motor inverter efficiency for this condition is 96.6% and DC/DC converter efficiency is 99.2%, higher electric power (10.8 kW) is needed to obtain 9 kW braking power on the shaft. To avoid even a slight overload of the fuel cell, energy lack (0.8 kW of power) is taken from the battery. Finally, 9 kW of braking power during horizontal flight is only a theoretical assumption and in a real flight, it may happen that 7 kW of braking power for horizontal flight is enough, or, in contrast, 11 kW is required. This is one of the reasons to extend the energy capacity of the electrochemical battery for the first tests. After real flight tests, the battery can be redesigned using smaller 10 Ah cells from the same family when braking power is lower than assumed, or the existing battery may be kept in the case in which higher braking power for horizontal flight will be required.

Taking into account horizontal flight point and assumed 9 kW of braking power, and noting that almost all energy is taken from the fuel cell and a negligibly small amount from the battery directly connected to the common DC bus, the efficiency in this point can be determined using (5b) with a prior determination of battery power and its efficiency in a given point (5a). Battery efficiency and total efficiency for climbing are calculated by (6a), and (6b) respectively, whereas for take-off stage by (7a) and (7b) respectively. For calculation purposes, maximum voltage battery was taken into consideration at a starting point with maximum braking power 37 kW, 380 V as the average voltage during take-off and climbing (33 kW of braking power) and nominal battery voltage 355 V during horizontal flight (9 kW of braking power). In all cases, the fuel cell power taken is maximal (i.e., rated). This is, of course, exemplary calculation and to find the total efficiency in each point (note that the battery voltage changes due to the discharging), the calculation should be made online along the lasting profile assumed.

$$\varepsilon_{BAT\_9\text{kW}} = \frac{(355\text{V})^2}{\left(\frac{9\text{kW}-10\text{kW}\cdot 0.992\cdot 0.966\cdot 0.87}{0.966\cdot 0.87}\right)\cdot 0.384\Omega + (355\text{V})^2} = 0.9976 \quad (5a)$$

$$\varepsilon_{t\_9\text{kW}} = \frac{9\text{kW}\cdot 0.9976\cdot 0.992\cdot 0.87}{9\text{kW} + 10\text{kW}\cdot 0.966\cdot 0.87\cdot (0.9976 - 0.992)} = \mathbf{0.856} \quad (5b)$$

$$\varepsilon_{BAT\_33\text{kW}} = \frac{(380\text{V})^2}{\left(\frac{33\text{kW}-10\text{kW}\cdot 0.992\cdot 0.976\cdot 0.94}{0.976\cdot 0.94}\right)\cdot 0.384\Omega + (380\text{V})^2} = 0.9352 \quad (6a)$$

$$\varepsilon_{t\_33\text{kW}} = \frac{33\text{kW}\cdot 0.9352\cdot 0.992\cdot 0.94}{33\text{kW} + 10\text{kW}\cdot 0.976\cdot 0.94\cdot (0.9352 - 0.992)} = \mathbf{0.886} \quad (6b)$$

$$\varepsilon_{BAT\_37\text{kW}} = \frac{(400\text{V})^2}{\left(\frac{37\text{kW}-10\text{kW}\cdot 0.992\cdot 0.976\cdot 0.945}{0.976\cdot 0.945}\right)\cdot 0.384\Omega + (400\text{V})^2} = 0.9324 \quad (7a)$$

$$\varepsilon_{t\_37\text{kW}} = \frac{37\text{kW}\cdot 0.9324\cdot 0.992\cdot 0.945}{37\text{kW} + 10\text{kW}\cdot 0.976\cdot 0.945\cdot (0.9324 - 0.992)} = \mathbf{0.887} \quad (7b)$$

From the above calculations, we can see that the higher the braking power, the higher the total efficiency. Even if the battery energy losses are relatively smaller (battery efficiency increases), the DC/AC converter efficiency decreases, and most importantly, motor efficiency decreases, which has the main influence on the total electrical energy conversion efficiency.

4. CAN Communication System and Control Structure

4.1. Communication System

The scheme of communication between components is shown in the next Section 4.2 together with the control structure. The communication system comprises three isolated CAN-buses. The first one (CAN1) integrates the battery, DC/AC and DC/DC power converters, and on-board computer, and this communication is matched to the CAN protocol of the battery management system. The second communication bus (CAN2) is completely independent and it integrates the DC/AC converter with a speed command lever. This is to avoid any influence of other components on the speed commanded from the lever as well as introduce a kind of redundancy in speed commanding. Simply, any failure in CAN1 does not influence speed commanding. Additionally, when CAN2 communication permanent failure is detected between the speed lever and power converter, CAN1 can be used for speed commanding from the on-board computer as an alternative commanded speed source.

The third bus (CAN3) is implemented between the on-board computer and the fuel cell controller. The fuel cell controller requires only starting and stopping commands, and besides these two signals, the fuel cell controller independently tackles the fuel cell state. However, the on-board computer is involved in some data collection of the whole system during the experiment, including some parameters of the fuel cell. CAN3 is established separately from CAN1 and CAN2 because the fuel cell system has been elaborated by another team in the project [12]. In such a case it is easier to coordinate the data transfer when only two devices are communicated in the same bus.

The on-board computer is responsible for the devices switching on before take-off, collection of all data during profile realization, visualization, and device switching off after profile ending. Control of energy transfers from the fuel cell and battery to the electric motor is made in the power converter controllers without intervention of the on-board computer. The on-board computer was additionally connected to a single-chip computer RaspberryPi 3B+, to send the data by Wi-Fi to the mobile phone placed on-board, and further by GSM to the webpage. It allows for observation of the waveforms on-line on a PC computer during testing of the motor glider on the runway.

4.2. Scheme of the Control System for Power Converters

A detailed scheme of the control and communication structure of power electronic converters set for the hybrid energy system with a fuel cell and battery is shown in Figure 7. The DC/AC converter feeding motor is equipped with stator current vector control, in which the d component of the current vector is set to zero, because the machine does not require field strengthening to obtain the maximum demanded power. The q component of the current vector responsible for torque creation is referenced from the outer speed controller. This part is a classical rotor flux-oriented control. The reference speed is commanded from the CAN communicated speed command lever. All controllers are proportional-integral type. A saturation block joined with a mechanical speed controller $\mathrm{Rn_m}$ is a reference current limiter and also serves as the anti-wind-up structure for the speed controller.

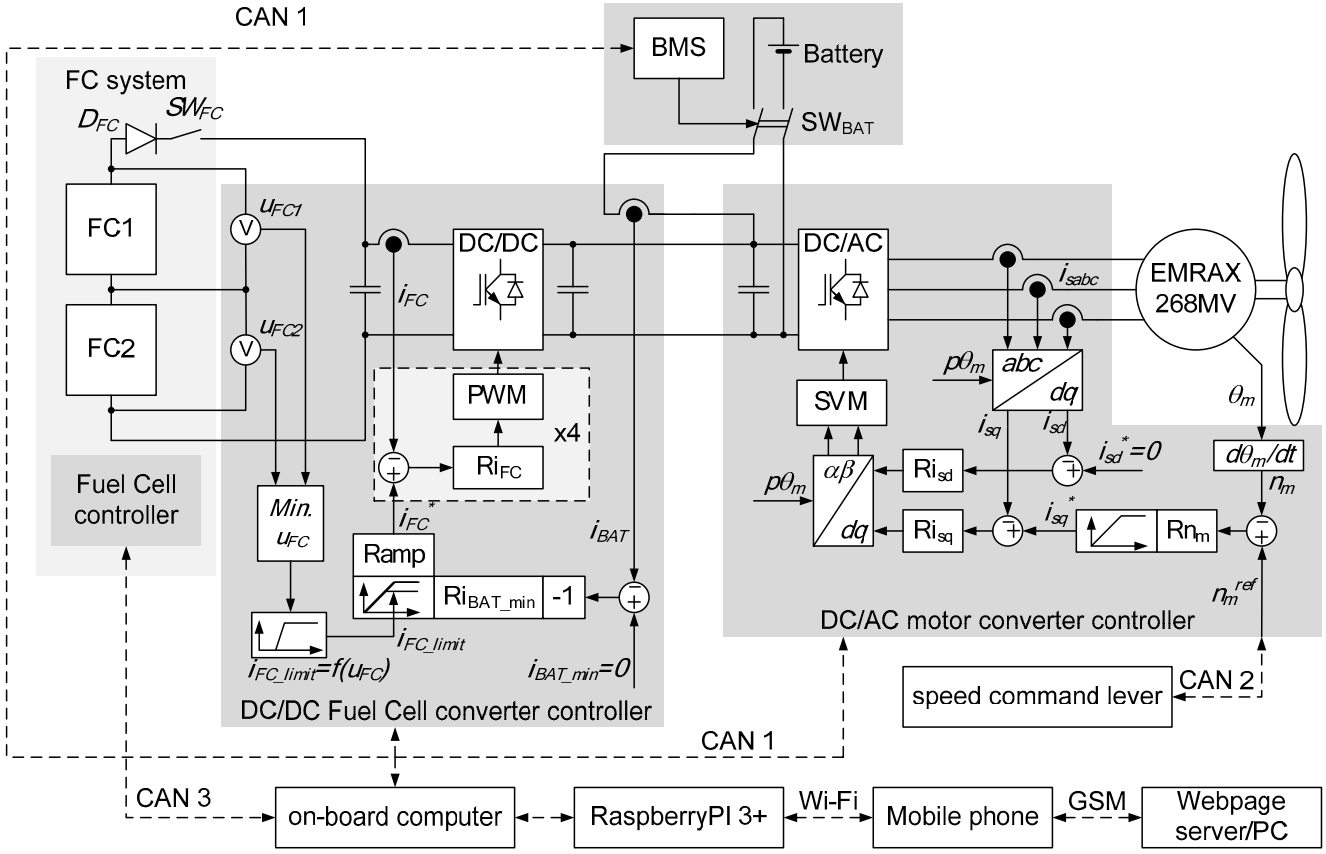

Figure 7. Detailed control and communication structure of the power conversion system in a hybrid fuel cell and battery-based electric drive for the AOS-H2 motor glider.

The basic control of the fuel cell converter is composed of four current regulators, each for a single branch of the DC/DC interleaved converter. The reference value i_{FC}* of the fuel cell current is divided by four to obtain the same reference for each single current regulator. Four independent current sensors are also used to measure the currents in each inductor of the interleaved converter.

4.3. Battery Charging Current Regulator

Charging of the battery during flight is not taken into consideration for the elaborated alternative communication-less method even if the power possible from the fuel cell is higher than the instantaneous power consumption by the motor drive. This is because the charging process is less efficient and higher thermal losses occur in a considerably high charging current. When the propeller is not used during flight of the glider, the full power of the fuel cell (10 kW) can be used for battery charging. This is equivalent to 1.5C of charging current. Taking into account that in the initial stage of the profile, we have 30 kW of battery power discharge, and the temperature of cells increases by 14 °C, further charging may increase the cells temperature to over 45 °C. According to the cells specification in the temperature range 35–45 °C the charging current should be limited to 1C, whereas above 45 °C charging is prohibited at all. As during CAN communication fault no information from battery BMS can be received by other devices, the temperature of cells is unknown. Thus, we decided to resign from the charging process when the presented alternative communication-less control method is used. To avoid charging during energy surplus in the fuel cell, the reference fuel cell current i_{FC}* is reduced by the battery charging current controller Ri_{BAT_min} in the DC/DC converter control structure. Implementation of battery charging is simply possible by a change of the minimum current value i_{BAT_min} to some allowed level (negative value).

4.4. Fuel Cell Undervoltage Protection

Series connected fuel cell stacks are periodically short-circuited to improve the humidification of the cell, which positively influences stacks performances and consequently increases the available power. Short circuits are made through additional switches SW1 and SW2 (Figure 5) during ten milliseconds with ten seconds intervals at each stack. Due to the series connection of two stacks, the total voltage on the fuel cell terminals during short circuit drops by half. Thus, energy flow is possible from the non short-circuited stack during this process. The other solution is to bring the fuel cell current to zero. Both manners are possible in DC/DC converter control, as shown in Figure 8.

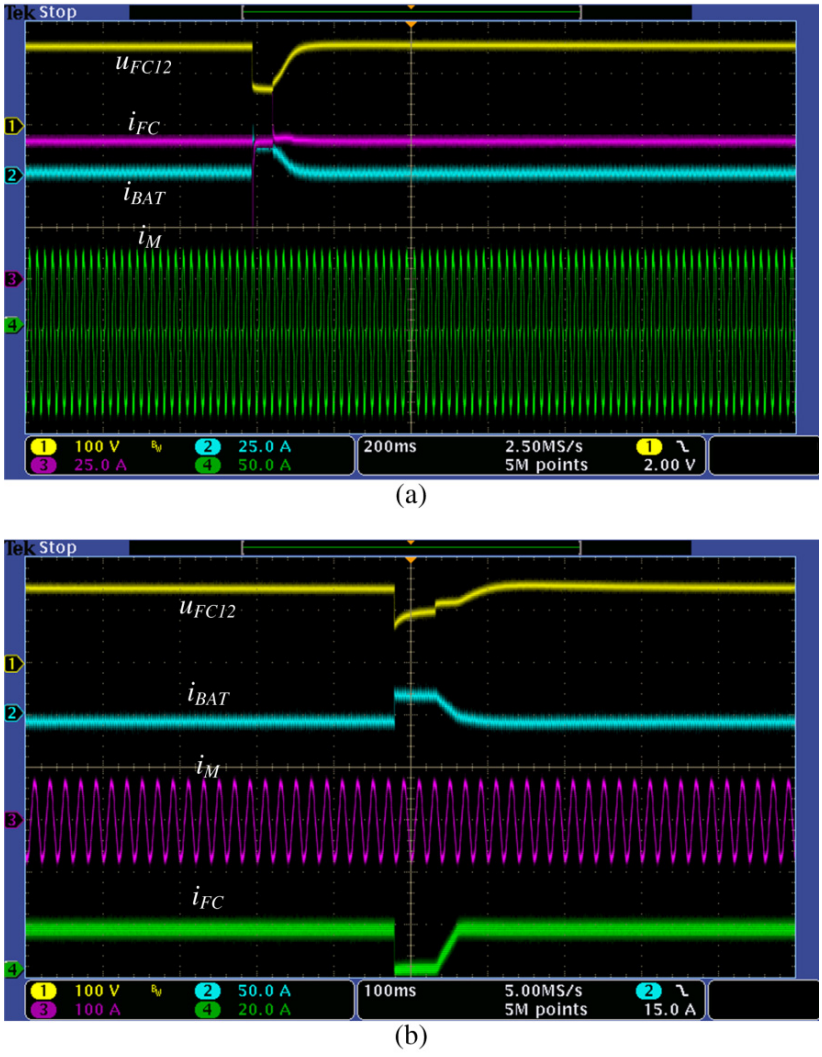

Figure 8. Possible behavior of the DC/DC converter during fuel cell short-circuit, (**a**) with loading and (**b**) with unloading, u_{FC12}-fuel cell total voltage, i_{FC}-fuel cell current, i_{BAT}-battery current, i_M-motor phase current.

Finally, to avoid additional loading of the fuel cell during short circuit in further research, the second solution has been taken into consideration, and this is realized by an additional function $i_{FC\_limit} = f(u_{FC})$ in the DC/DC converter control structure (Figure 7). The function is implemented for additional reduction of the fuel cell current limit, and the function details are shown in Figure 9. Periodical drop of the fuel cell current to zero causes increased current consumption by the battery. To avoid disconnection of the battery during fuel cell periodical short-circuiting, the battery over-current protection is realized in such a

way that five consecutive average values of battery current calculated in 100ms periods are compared with the current limit.

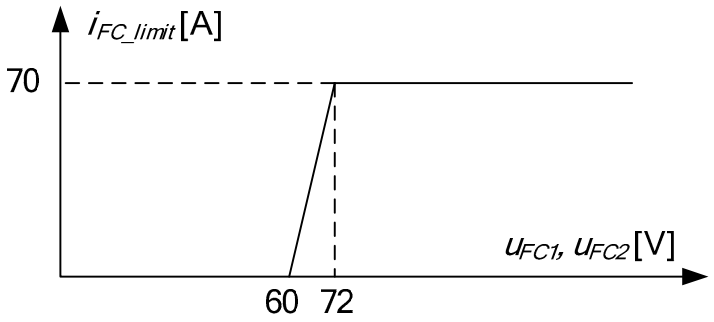

Figure 9. Fuel cell under-voltage protection function $i_{FC\_limit} = f(u_{FC})$.

The fuel cell under-voltage function serves as additional protection. The fuel cell current is reduced not only during short-circuit, but also in the case in which fuel cell operates above nominal point, and the fuel cell voltage dangerously drops below nominal value. To avoid fuel cell overload, this function is responsible for unloading the fuel cell system. This way, even if it is impossible to reach the rated power from the fuel cell, it operates with partial power, which is better than fuel cell system disconnection or even possible degradation of cells. A small supercapacitor bank can be of interest as additional storage assisting in the fuel cell short circuits. A supercapacitor bank connected in parallel to the input terminals of the DC/DC converter can be used to avoid battery current peaks during fuel cell short circuit. However, this requires an additional small power converter for charging of the supercapacitors bank in the intervals between short circuits and increases the weight of the conversion system by ca. 3 kg.

4.5. Discussion on Other Possible Faults in the Energy Conversion System

Possible faults may happen in all devices. It is quite difficult to find a solution giving DC/AC converter postfault or motor postfault operation in the used configuration. This is why the motor is sized with some margin, avoiding overheating during take-off and climbing, and the same is true of the DC/AC converter power modules selection. Some protections to avoid faults, such as prevention against motor or DC/AC converter temperature increase, can be done by reducing maximum torque in the DC/AC converter controller. To obtain higher reliability, multiphase (more than three phases) machines with DC/AC converter redundant legs may be used, or two independent machines clutched on the same shaft and fed from two independent DC/AC converters. However, taking into account that the system is designed for a glider, such issues are not critical.

Possible fuel cell system faults cause reduction of available electric power, and the battery only provides energy in this state. Its ability depends on the available energy in a battery, which depends on the stage of flight. In the case of fuel cell system fault, the information from the fuel cell controller or DC/DC converter controller is provided to the on-board computer by one of the CAN communication channels and the available power for the DC/AC converter can be recalculated to the maximum possible torque/speed on the motor shaft. The information of recalculated maximum torque/speed is updated in the DC/AC converter controller. The new maximum torque/speed may be available up to the total discharge of the battery.

Battery faults can be assisted in a similar way. Battery fault detection and its disconnection from the DC bus through the battery switch SW_{BAT} is done by BMS. After disconnection of the battery by BMS, information about it can be sent to the on-board computer and the maximum torque/speed is updated by an on-board computer in the DC/AC converter controller. In such a case, additionally, action is needed related to the DC bus maximum voltage control in the case in which the propeller energy demand is lower than the energy fed from the fuel cell. In such a case, the adaptive current limitation of the fuel cell must be enabled to limit the fuel cell instantaneous power when DC voltage reaches 400V. These issues are part of further research.

5. Experimental Tests in Stationary Conditions

Stationary conditions experimental test results are obtained with a fuel cell simulator to test the operation of the power conversion system. A fuel cell simulator is not intended to reproduce the model of chemical processes, but to emulate electrical voltage in the DC/DC converter input terminals with consideration of stack short-circuit processes. The simulator voltage is set constant at the level adequate to the nominal power. This means that the full nominal characteristic of the fuel cell is not implemented; only the nominal operating point is implemented. Figure 10 presents the waveforms of voltages and currents in the power conversion system during the assumed profile realization.

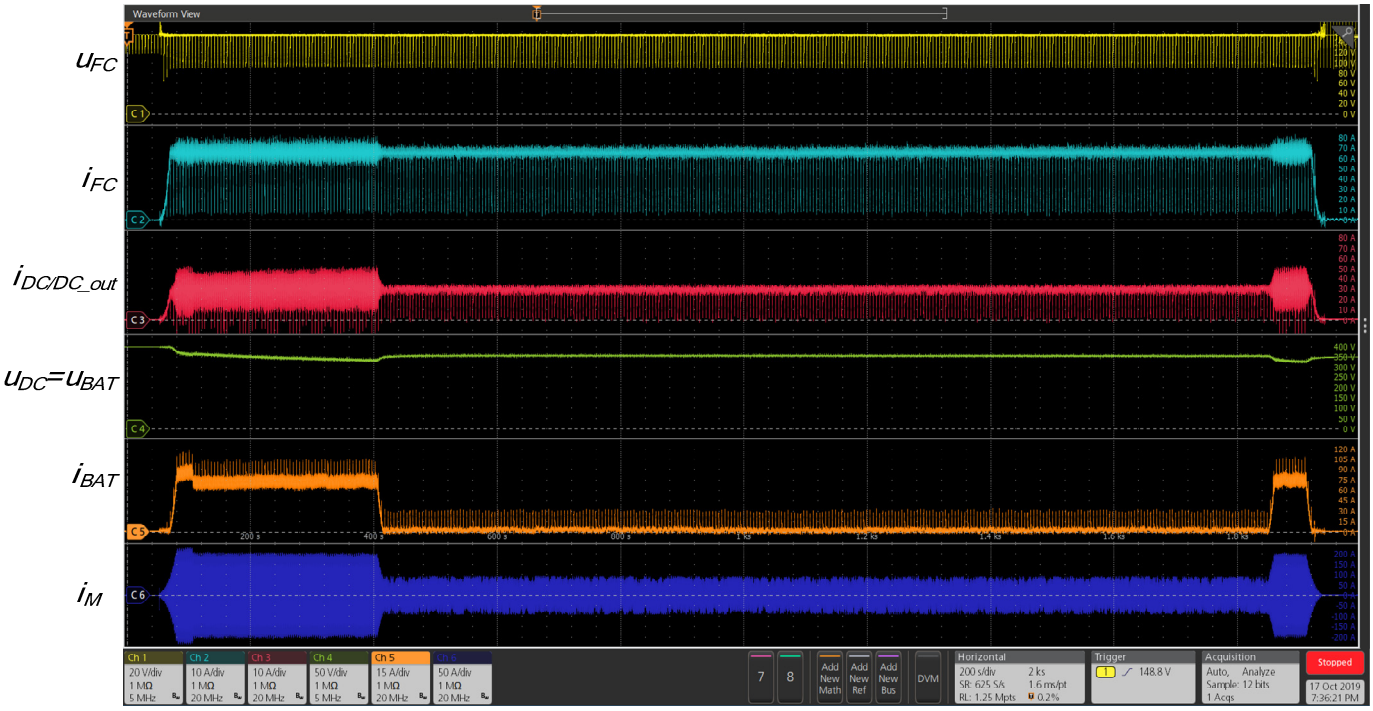

Figure 10. Selected waveforms from the stationary condition tests during realization of mission profile registered by an oscilloscope.

Corresponding results presenting powers, electric motor torque, and speed are shown in Figure 11. It can be observed in both figures (Figures 10 and 11) that during fuel cell any stack short circuit, the fuel cell current drops to zero, and the battery current increases, climbing above the 100 A battery current limit, but it does not cause disconnection of the battery. It can also be observed that during motor start-up and at the end of profile when the motor power is lower than the fuel cell nominal power, the battery charging is avoided due to the additional battery charging controller Ri_{BAT_min}.

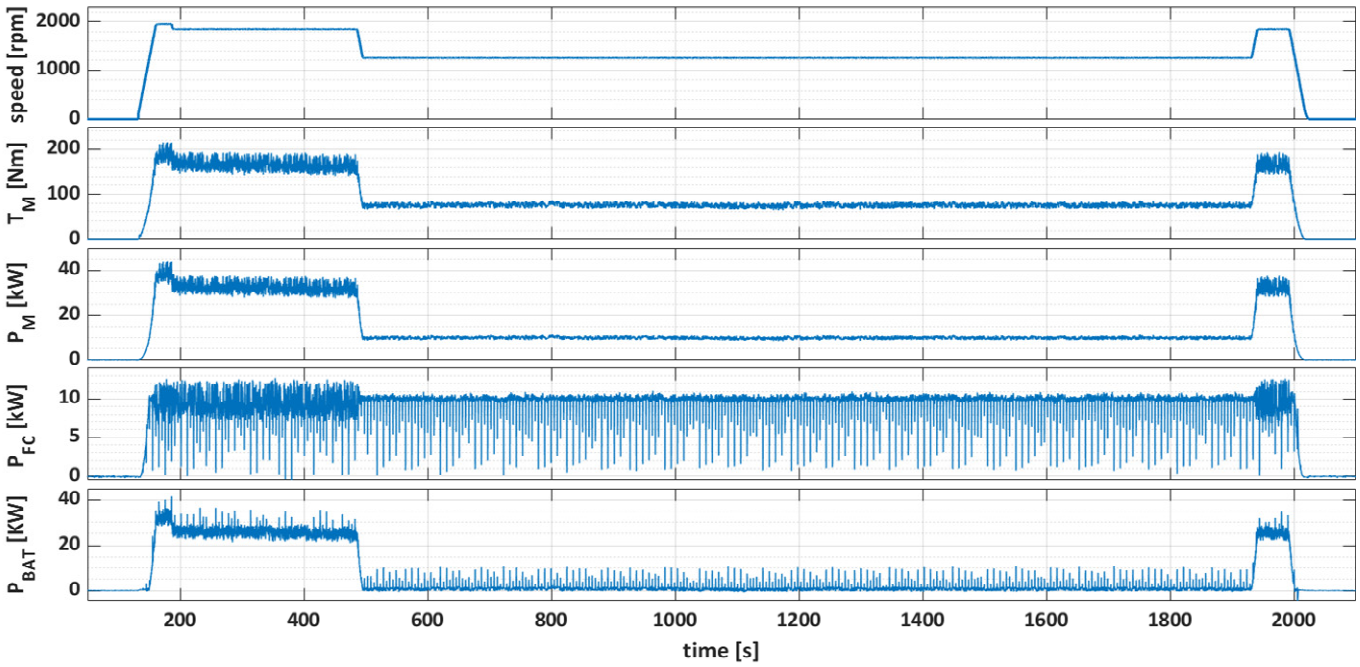

Figure 11. Selected waveforms from the stationary condition tests during realization mission profile registered by DSP controllers.

6. Experimental Tests of Aircraft on a Runway

Experimental tests of the aircraft with a hybrid fuel cell/battery-based drive system were done on a runway in the Aviation Training Centre of Rzeszow University of Technology, Poland. The picture of the motor glider on a runway is shown in Figure 12. The aircraft velocity equal to 80 km/h assuring climbing was achieved after 17 s in the test, in which before running the pilot waited to reach full motor speed and power before hand-brake release.

Figure 12. The AOS-H2 motor glider on the runway of the Aviation Training Centre of Rzeszow University of Technology.

Unfortunately, due to the lack of national rules related to hydrogen use in manned flying platforms, full flight tests were not permitted. However, the results of running the aircraft on a runway show some properties of the hybrid drive. The tests were done in spring conditions with very low air temperature (ca. 5 °C), thus the performance of the

hybrid drive was limited in relation to the assumptions. The maximum power of the fuel cell system (which could be obtained during this short test without a significant voltage drop above the nominal level) was 7.5 kW, so the maximum total electric power equal to 37 kW was achieved. To achieve higher temperature of the fuel cell stacks allowing fuel cell rated power and assuming 40 kW of total power, longer tests are required at this low ambient temperature (longer start-up process of the fuel cell to increase the temperature of cells). Nevertheless, 37 kW of available total electric power allowed the aircraft to achieve the speed needed to start climbing. The results of the tests on the runway collected using RaspberryPI 3+, a mobile phone, and GSM communication are shown in Figure 13.

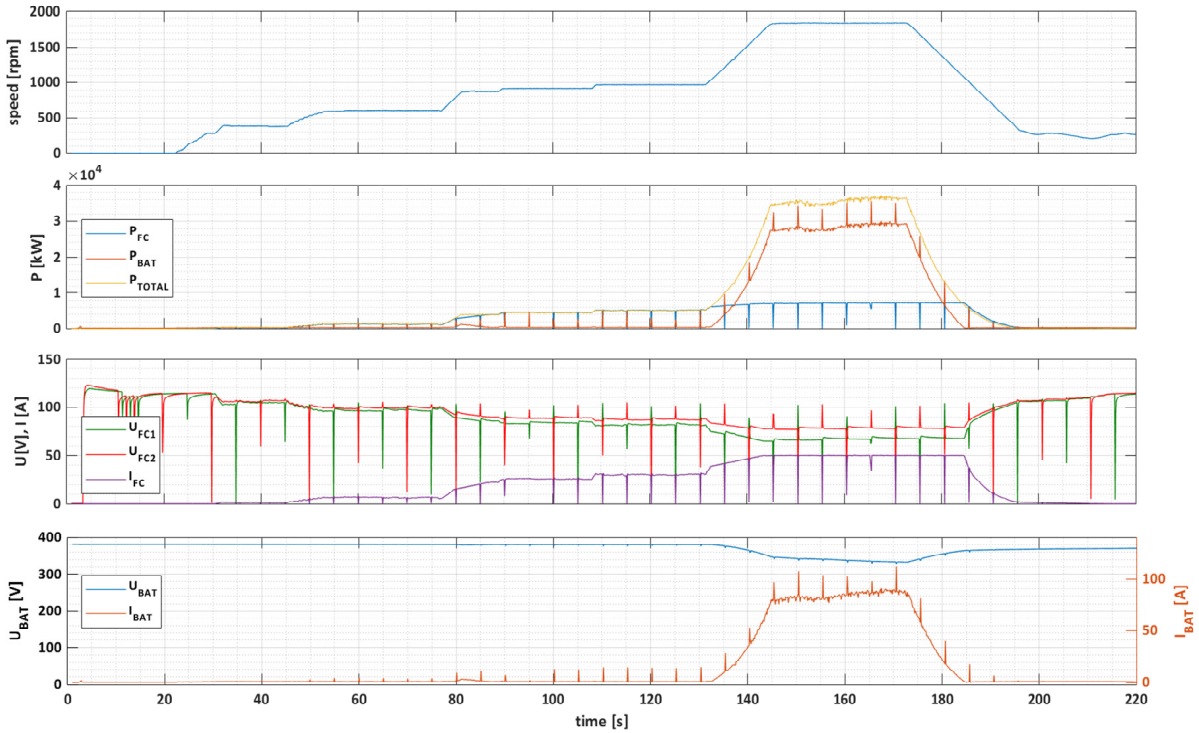

Figure 13. Selected results from the motor glider tests on the runway.

7. Conclusions

The paper presents realization of a power conversion system and its control for a hybrid fuel cell and battery-based drive system for a light aircraft; its properties were examined in stationary and limited non-stationary tests. The motor power converter was built using IGBT technology, whereas the DC/DC converter was constructed using SiC technology. All components of the hybrid system (battery, converter, fuel cell controller, speed command lever, on-board computer) were connected using CAN communication. The main assumption of the control was to develop a control method not involving communication buses between components. This is to avoid possible faults of communication and possible delays in communication. The power conversion system is protected against charging of the battery, which is not recommended in the designed system, when the loading power is smaller than the possible power of the fuel cell. The control system takes into consideration fuel cell stacks periodically short circuiting, increasing humidification of cells. The control system protection ability has been proven in laboratory tests results in stationary conditions as well as during run-up of the motor glider on a runway.

Author Contributions: Conceptualization, G.I.; methodology, T.M.; software, T.M.; validation, G.I.; formal analysis, T.M. and G.I.; investigation, T.M., G.I., M.N.; resources, T.M. and M.N.; data curation, T.M.; writing—original draft preparation, G.I.; writing—review and editing, T.M. and M.N.; visual-

ization, T.M.; supervision, G.I.; project administration, G.I.; funding acquisition, G.I. All authors have read and agreed to the published version of the manuscript.

Funding: This research was funded by The National Centre for Research and Development, grant number PBS3/A6/24/2015, and the APC was funded by the Warsaw University of Technology within the IDUB-Open Science Program.

Data Availability Statement: No new data were created or analyzed in this study. Data sharing is not applicable.

Acknowledgments: The authors wish to thank the teams co-working within the project for successful cooperation:

- the team from the Institute of Aviation and Applied Mechanics of the Warsaw University of Technology led by Professor Piotr Czarnocki, responsible for airframe design,
- the team from the AGH University of Science and Technology in Cracow, led by Professor Magdalena Dudek, responsible for fuel cell system designing, building and running.
- the team from Rzeszow University of Technology (project Leader) led by Professor Marek Orkisz, and
- Henryk Mynarski, the owner of The Glider Factory "Jeżów" responsible for the airframe building.

Conflicts of Interest: The authors declare no conflict of interest. The funders had no role in the design of the study; in the collection, analyses, or interpretation of the data; in the writing of the manuscript, or in the decision to publish the results.

References

1. Lapena-Rey, N.; Mosquera, J.; Bataller, E.; Orti, F. First fuel-cell manned aircraft. *J. Aircr.* **2010**, *47*, 1825. [CrossRef]
2. Romeo, G.; Borello, F.; Correa, G.; Cestino, E. Flight test Validation of the Dynamic Model of a Fuel Cell System for Ultra-Light Aircraft. *J. Aerosp. Eng.* **2015**, *229*, 917.
3. Bradley, T.H.; Moffitt, A.; Mavris, D.N.; Pavekh, D.E. Development and experimental characterization of a fuel cell powered aircraft. *J. Power Sources* **2007**, *171*, 793. [CrossRef]
4. Niu, C.; Lee, H.; Chen, S.; Li, Q.; Du, J.; Xu, W.; Zhang, J.-G.; Whittingham, M.S.; Xiao, J.; Liu, J. High-energy lithium metal pouch cells with limited anode swelling and long stable cycles. *Nat. Energy* **2019**, *4*, 551. [CrossRef]
5. Kadyk, T.; Winnefeld, C.; Hanke-Rauschenbach, R.; Krewer, U. Analysis and Design of Fuel Cell Systems for Aviation. *Energies* **2018**, *11*, 375. [CrossRef]
6. Nishizawa, A.; Kallo, J.; Garrot, O.; Weiss-Ungethüm, J. Fuel cell and Li-ion battery direct hybridization system for aircraft applications. *J. Power Sources* **2013**, *222*, 294. [CrossRef]
7. Huangfu, Y.; Guo, L.; Ma, R.; Gao, F. An Advanced Robust Noise Suppression Control of Bidirectional DC–DC Converter for Fuel Cell Electric Vehicle. *IEEE Trans. Transp. Electrif.* **2019**, *5*, 1268. [CrossRef]
8. Zhang, Y.; Zhang, C.; Huang, Z.; Xu, L.; Liu, Z.; Liu, M. Real-Time Energy Management Strategy for Fuel Cell Range Extender Vehicles Based on Nonlinear Control. *IEEE Trans. Transp. Electrif.* **2019**, *5*, 1294. [CrossRef]
9. Flynn, M.; Jones, C.E.; Norman, P.J.; Burt, G.M. A Fault Management-Oriented Early-Design Framework for Electrical Propulsion Aircraft. *IEEE Trans. Transp. Electrif.* **2019**, *5*, 465. [CrossRef]
10. Flynn, M.; Sztykiel, M.; Jones, C.; Norman, P.; Burt, G.; Miller, P.; Husband, M. Protection and Fault Management Strategy Maps for Future Electrical Propulsion Aircraft. *IEEE Trans. Transp. Electrif.* **2019**, *5*, 1458. [CrossRef]
11. Horizon Fuel Cell H-5000 User Manual. Available online: https://7782216e-8aad-4387-b6a4-b13b0ab6b227.filesusr.com/ugd/047f54_fa621f546cf74b42451427facb47179c.pdf (accessed on 18 February 2021).
12. Dudek, M.; Raźniak, A.; Rosół, M.; Siwek, T.; Dudek, P. Design, Development, and Performance of a 10 kW Polymer Exchange Membrane Fuel Cell Stack as Part of a Hybrid Power Source Designed to Supply a Motor Glider. *Energies* **2020**, *13*, 4393. [CrossRef]
13. Gupta, G.; Wu, B.; Mylius, S.; Offer, G.J. A systematic study on the use of short circuiting for the improvement of proton exchange membrane fuel cell performance. *Int. J. Hydrog. Energy* **2017**, *42*, 4320. [CrossRef]
14. Frosina, E.; Senatore, A.; Palumbo, L.; Di Lorenzo, G.; Pascarella, C. Development of a Lumped Parameter Model for an Aeronautic Hybrid Electric Propulsion System. *Aerospace* **2018**, *5*, 105. [CrossRef]
15. Emrax 268MV Datasheet. Available online: https://emrax.com/wp-content/uploads/2017/01/emrax_268_technical_data_4.5.pdf (accessed on 18 February 2021).
16. Kimura, T.; Saitou, R.; Kubo, K.; Nakatsu, K.; Ishikawa, H.; Sasaki, K. High-power-density Inverter Technology for Hybrid and Electric Vehicle Applications. *Hitachi Rev.* **2014**, *63*, 96.
17. Zdanowski, M.; Rąbkowski, J.; Barlik, R. Highly-Efficient and Compact 6kW/4×125 kHz Interleaved DC-DC Boost Converter with SiC Devices and Low-Capacitive Inductors. *Energies* **2017**, *10*, 363. [CrossRef]

18. Warncke, M.; Fahlbusch, S.; Hoffmann, K.F. DC/DC-Converter for Fuel Cell Integration in More Electric Aircraft Applications. In Proceedings of the European Conference on Power Electronics and Applications (EPE'17 ECCE Europe), Warsaw, Poland, 11–14 September 2017; pp. P.1–P.10.
19. Zhuo, S.; Gaillard, A.; Li, Q.; Ma, R.; Paire, D.; Gao, F. Current Ripple Optimization of Four-Phase Floating Interleaved DC–DC Boost Converter Under Switch Fault. *IEEE Trans. Ind. Appl.* **2020**, *56*, 4214. [CrossRef]